**Supplementary Material:**

# Strategic synthesis of sponge-like structured $SiO_x$@C@CoO multifunctional composites for high-performance and stable lithium-ion batteries

Pu Wang[a], Zhongti Sun[b], Hui Liu[c], Zhi-Wen Gao[c], Jianguo Hu[a], Wan-Jian Yin[d], Qingqing Ke[a,*], Hugh Lu Zhu [a,*]

[a] School of Microelectronics Science and Technology, Sun Yat-sen University, Zhuhai 519082, China
* Corresponding authors
Email: *zhulu5@mail.sysu.edu.cn; keqingq@mail.sysu.edu.cn*

[b] School of Materials Science and Engineering, Jiangsu University, Zhenjiang 212013, P. R. China

[c] Department of Electrical and Electronic Engineering, The University of Hong Kong, Hong Kong 999077, SAR China

[d] College of Energy, Soochow Institute for Energy and Materials InnovationS (SIEMIS), and Jiangsu Provincial Key Laboratory for Advanced Carbon Materials and Wearable Energy Technologies, Soochow University, Suzhou 215006, China

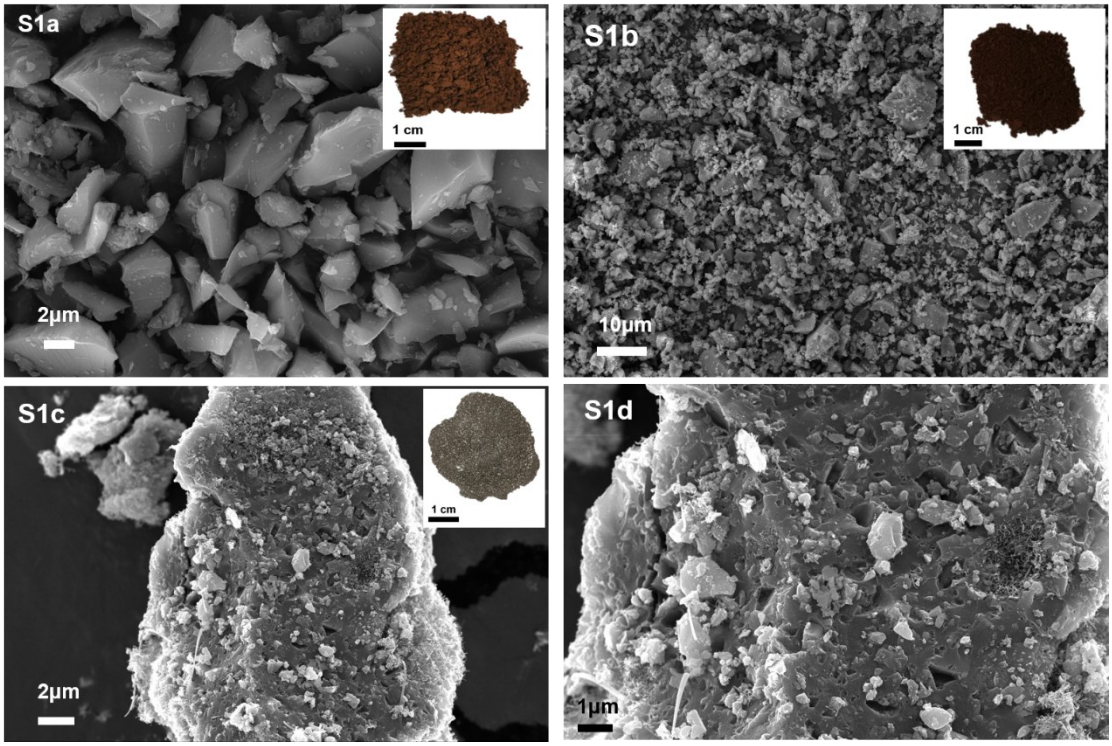


Figure. S1: SEM images of SiO particles (a) before ball milled (inside: Photograph SiO power before ball milled); (b) after ball milled (inside: Photograph SiO power after ball milled); SEM images of $SiO_x$@C particles at (c) low (inside: Photograph $SiO_x$@C power after calcination process) and (d) high magnifications.

As can be seen from Figure S1a, commercial SiO is an obvious block structure. And there is a decrease in particle sizes of SiO after the ball milling process, although the morphology of the block remained (Figure S1b). After spray drying with sucrose, the morphology of small particles attached to the surface of $SiO_x$ can be observed in Figure S1c. Sucrose molecules are decomposed into carbon adsorbed on the surface of $SiO_x$ during the sintering process, and finally form $SiO_x$@C nanoparticles, which are shown in Figure S1d.

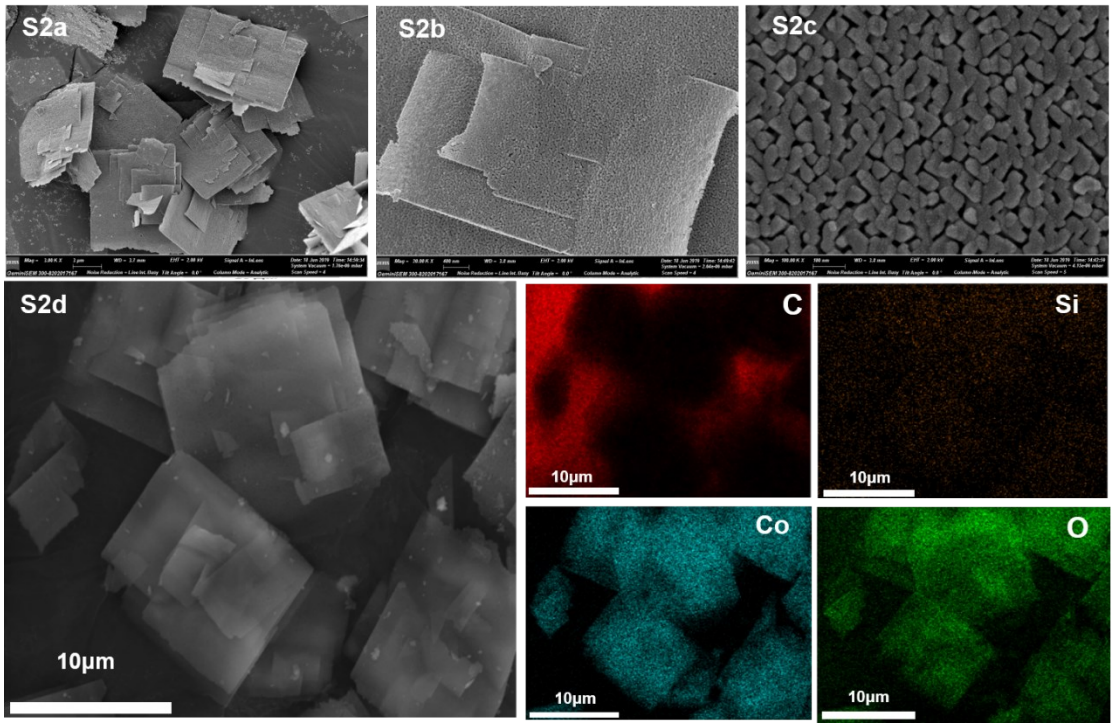


Figure. S2: SEM images of CoO nanosheets at (a) low and (b) (c) high magnifications, (d) SEM images and the corresponding EDX elemental mappings of C, Si, O and Co in CoO nanosheets.

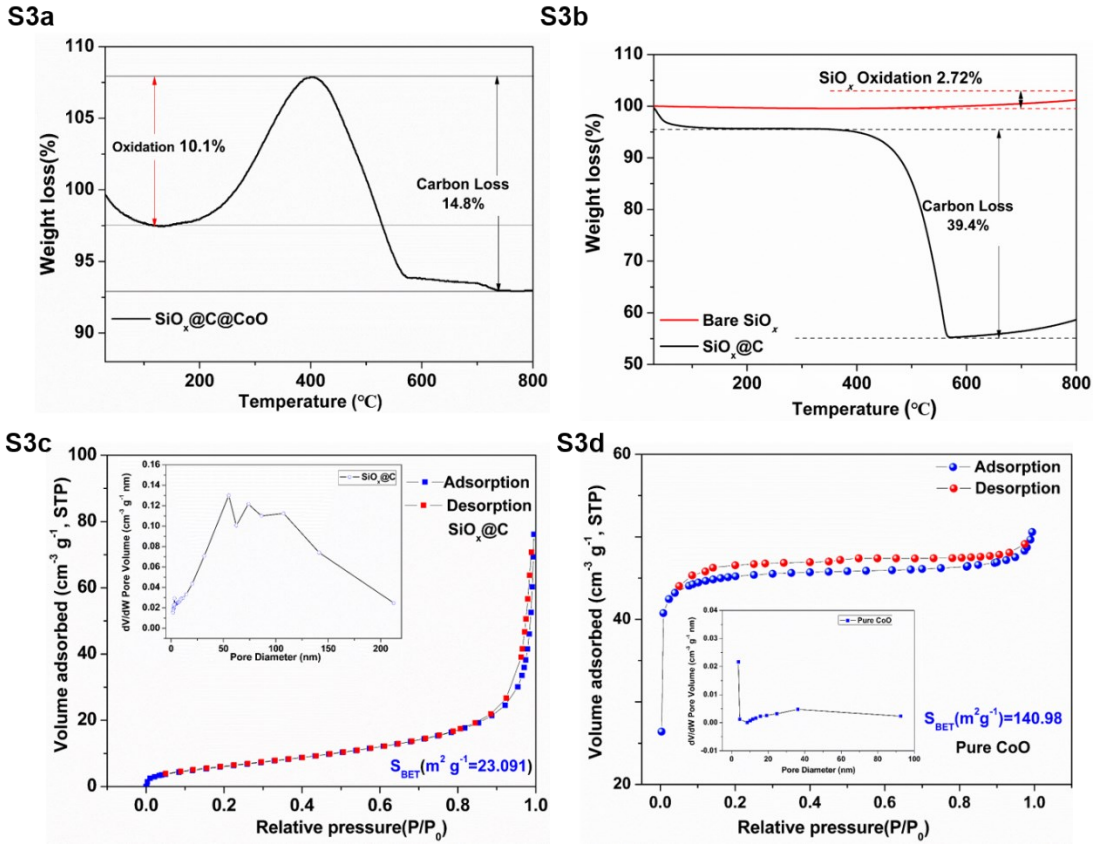


Figure S3: (a) TGA curves of $SiO_x$@C@CoO; (b) TGA curves of $SiO_x$@C and bare $SiO_x$ (red) (c) $N_2$ adsorption/desorption isotherms curve of the $SiO_x$@C (inside: pore size distribution profile); (d) $N_2$ adsorption/desorption isotherms curve of the Pure CoO (inside: pore size distribution profile).

**S4**

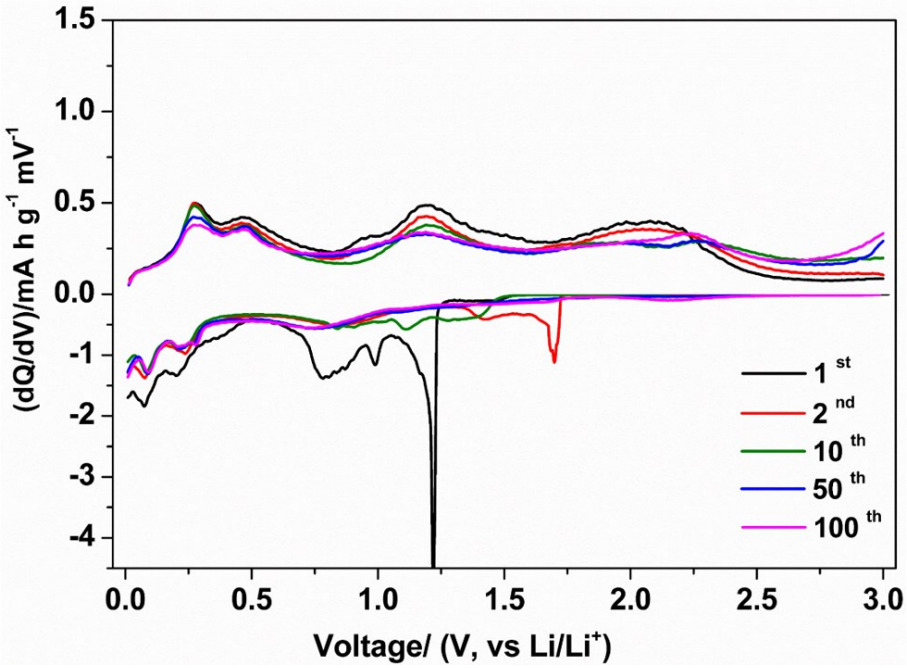


Figure S4: Differential capacity plot of $SiO_x$@C@CoO electrode.

**Table S1: Comparison of rate capacity retention of $SiO_x$-based materials between this work and the previous reports.**

| Composite | Current ($A\ g^{-1}$) | Voltage range (V) | Reversible capacity ($mA\ h\ g^{-1}$) | Mass Loading ($mg\ cm^{-2}$) | Ref. |
|---|---|---|---|---|---|
| **SiOC** | 3.2 | 0.01-3 | 290 | – | S1 |
| **$SiO_x$–$TiO_2$@C** | 6.4 | 0.01-2.5 | 375 | 1.3 | S2 |
| **$SiO_x$/C** | 5 | 0.01-3 | 303 | 1.5 | S3 |
| **$SiO_x$/C** | 1 | 0.01-3 | 423 | 2.3 | S4 |
| **$SiO_x$/graphene** | 5 | 0.01-1.5 | 190 | – | S5 |
| **FeSi/Si/$SiO_x$** | 5 | 0.01-1.5 | 333 | 1.1 | S6 |
| **Si/$SiO_x$@CNF** | 5 | 0.01-3 | 272 | – | S7 |
| **N-doped carbon/$SiO_x$** | 1.6 | 0.005-3 | 447 | 1.6-2.0 | S8 |
| **ternary $SiO_x$** | 5 | 0.01-3 | 406 | 0.53 | S9 |
| **$SiO_x$@C@CoO** | 5 | 0.01-3 | 484 | 1.5 | This work |

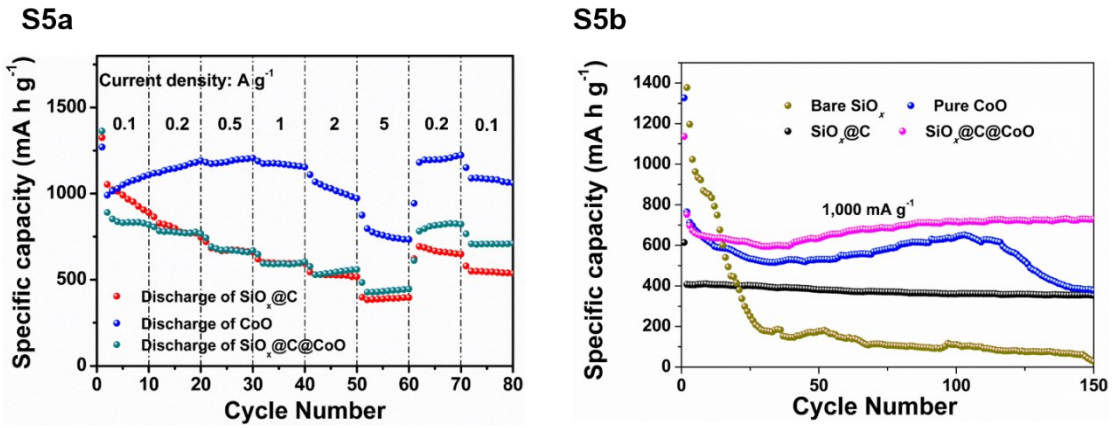


Figure S5: (a) Comparison of the rate performance of $SiO_x$@C, CoO, and $SiO_x$@C@CoO; (b) Comparative cycle performance of $SiO_x$, $SiO_x$@C, CoO and $SiO_x$@C@CoO at the current density of 1 A $g^{-1}$.

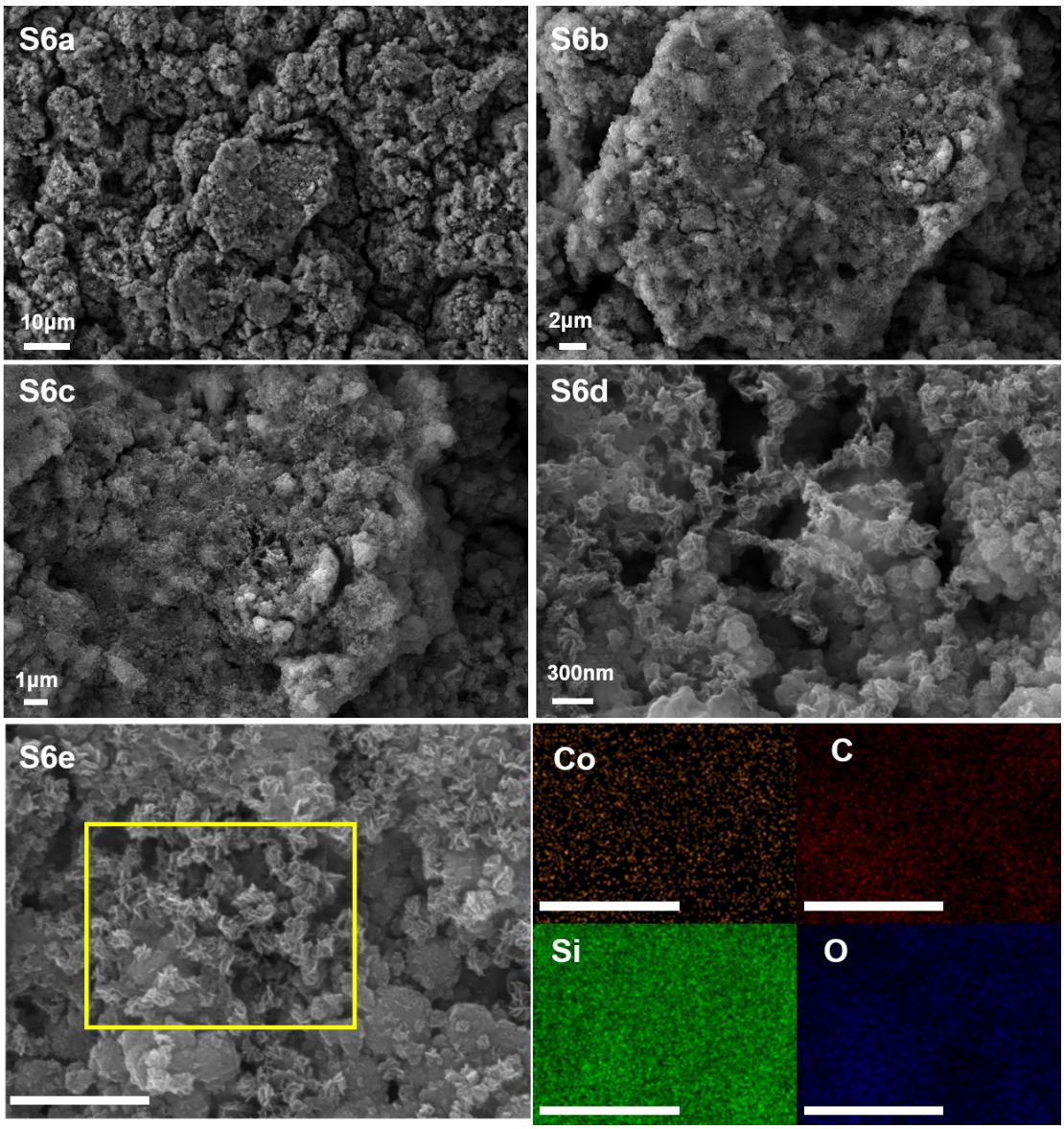


Figure S6: SEM images of $SiO_x$@C@CoO after 750 cycles at different scales (a) 10 μm; (b) 2 μm; (c) 1 μm; (d) 300 nm; (e) SEM images and the corresponding EDX elemental mappings of Co, C, Si, and O in $SiO_x$@C@CoO (scale bar 1 μm).

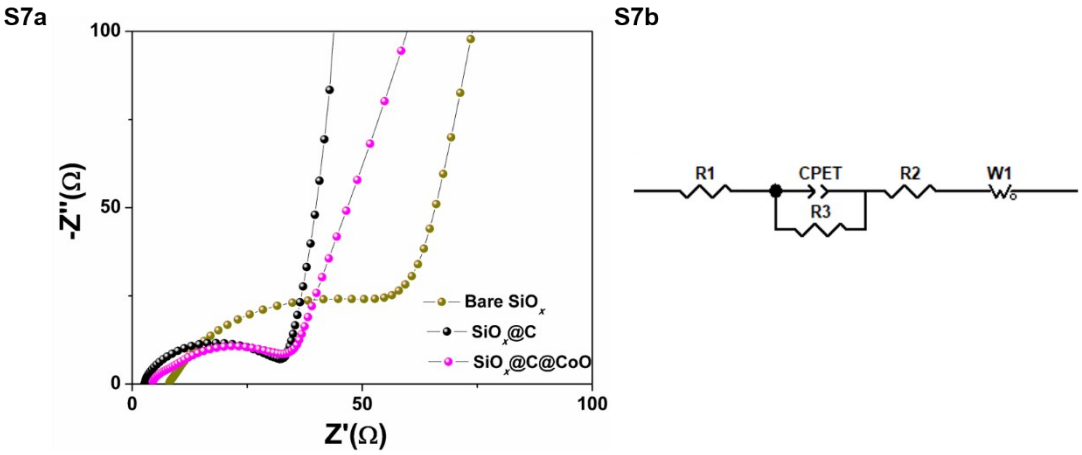


Figure S7: (a) EIS measurements of bare SiO, SiO$_x$@C, SiO$_x$@C@CoO; (b) the equivalent circuit of impedance spectra for fitting.

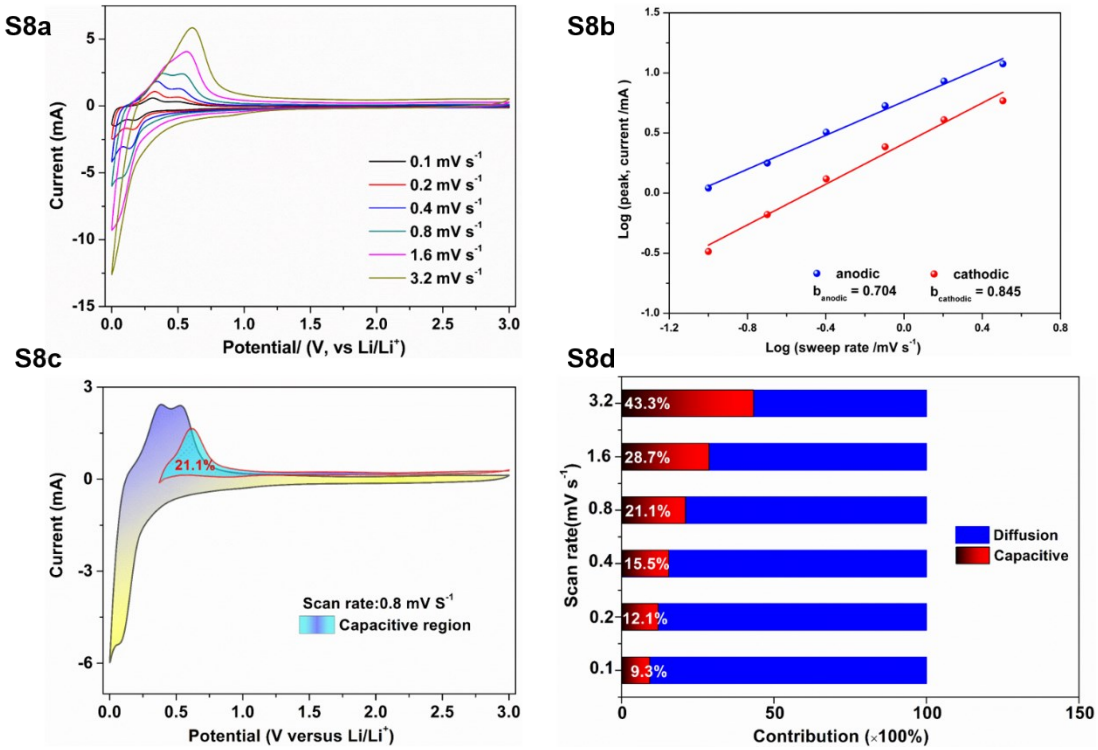


Figure S8: Kinetics analysis of the lithium storage behavior for the $SiO_x$@C electrode. (a) CV curves at different scan rates; (b) Log ($i$) versus log ($v$) plots at different cathodic/anodic peaks; (c) Capacitive and diffusion-controlled contribution to charge storage of sponge-like network at 0.8 mV $s^{-1}$; (d) Normalized contribution ratio of capacitance and diffusion at different scan rates.

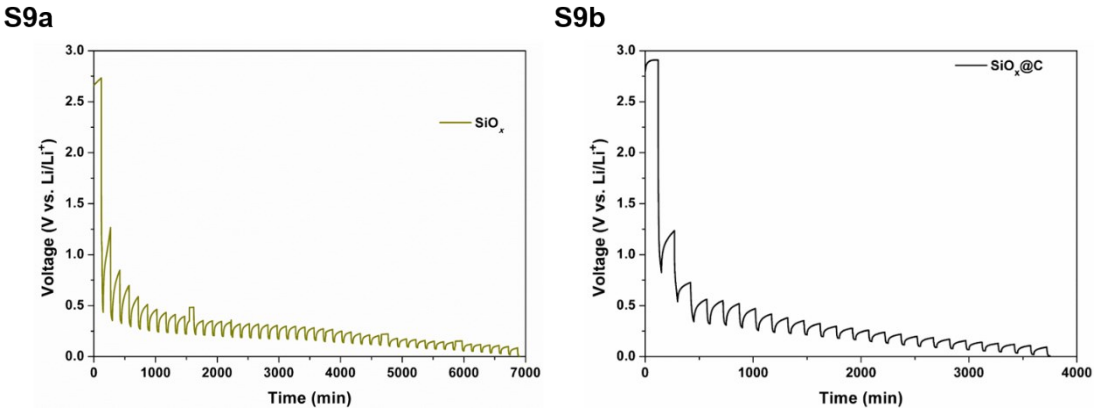


Figure S9: GITT curves of (a) $SiO_x$ and (b) $SiO_x$@C.

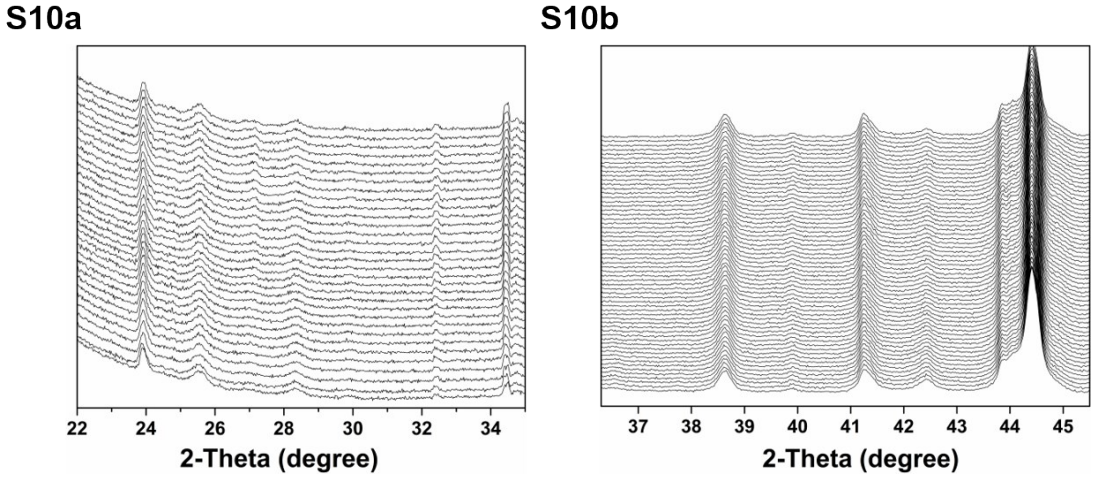


Figure S10: *In-situ* XRD patterns result for $SiO_x$@C@CoO at angles of (a) 22-35 degree and (b) 36.3-45.5 degree during discharging/charging processes for the initial two cycles.

S11

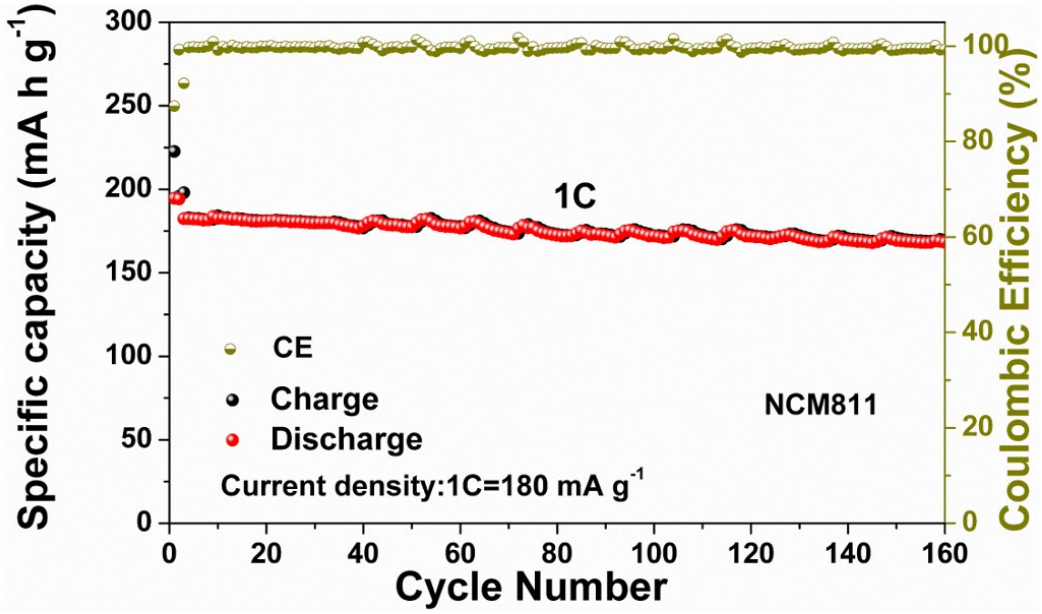


Figure S11: Cycling stability of the NCM811 electrode at 1 C.

**Table S2: Comparison of specific capacity of $SiO_x$@C@CoO sample with some other reported $SiO_x$-based electrode materials for LIBs.**

| Electrode Material | Reversible capacity (mA h $g^{-1}$) | Current density (mA $g^{-1}$) | Cycle number | Ref |
|---|---|---|---|---|
| N-$SiO_x$/C/GF-4 | 525.2 | 1000 | 500 | [S10] |
| $SiO_x$/C@graphite | 562 | 1000 | 300 | [S11] |
| rGO@$SiO_x$@C | 410 | 1000 | 200 | [S12] |
| ZIF@$SiO_x$ | 900 | 1000 | 350 | [S13] |
| SiOC | 701 | 100 | 100 | [S1] |
| $SiO_x$–$TiO_2$@C | 700 | 1000 | 600 | [S2] |
| $SiO_x$/C | 666.7 | 1000 | 400 | [S3] |
| $SiO_x$/C | 755 | 100 | 300 | [S4] |
| FeSi-Si/$SiO_x$ | 616 | 500 | 500 | [S6] |
| Si/$SiO_x$-CNF | 57.5 | 3000 | 1000 | [S7] |
| N dope C@$SiO_x$ | 623 | 1000 | 1000 | [S8] |
| $SiO_x$@C@CoO | 714 | 1000 | 750 | This work |

**Table S3: Comparison of Li diffusion coefficients of $SiO_x$@C@CoO samples with some other reported Si-based electrode materials for LIBs.**

| Electrode Material | Li diffusion coefficient ($cm^2\ s^{-1}$) | Mass Loading ($mg\ cm^{-2}$) | Ref |
|---|---|---|---|
| $SiO_x$–$TiO_2$@C | $8.2*10^{-14}$ | 1.3 | [S2] |
| $SiO_x$/$TiO_2$@MLG | $6.44*10^{-10}$ | 1.0 | [17] |
| $SiO_x$@$TiO_2$@C | $1.6*10^{-12}$ | 1.4 | [38] |
| N-$SiO_x$/C/GF-4 | $10^{-12}$~$10^{-9}$ | 0.8~1.2 | [S10] |
| ZIF@$SiO_x$ | $10^{-13}$~$10^{-10}$ | 0.9~1.1 | [S14] |
| Si | $10^{-12}$~$10^{-11}$ | ~ | [S15] |
| $SiO_x$ | $10^{-11}$~$10^{-12}$ | ~ | [S15] |
| $SiO_x$-hard carbon | $8.28\times10^{-10}$ | 0.5 | [S16] |
| $SiO_x$@C@CoO | $7.05\times10^{-8}$ | 1.5 | This work |

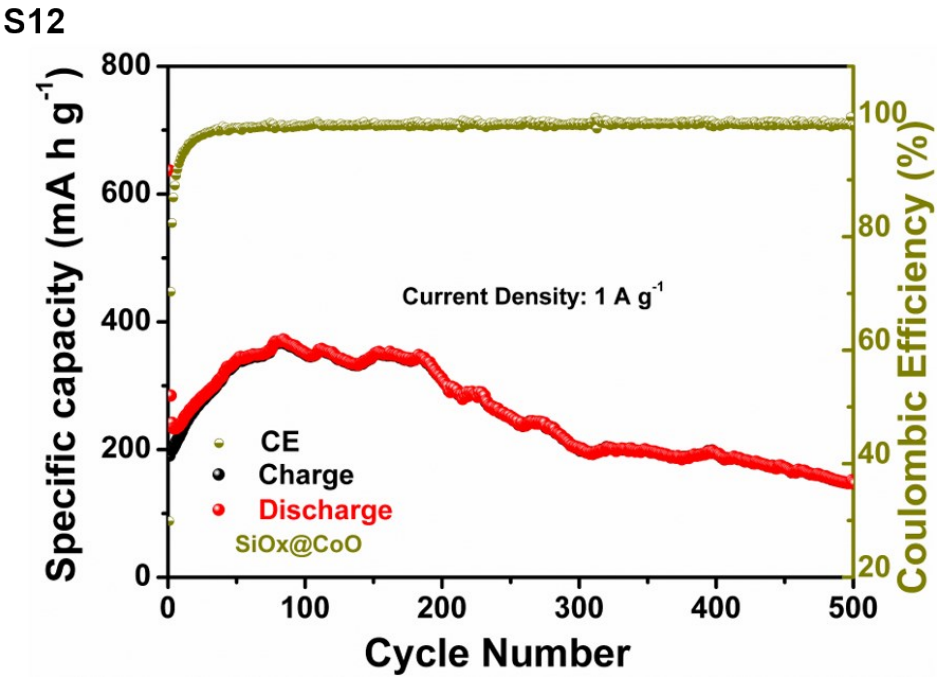


Figure S12: Cycling profiles of the $SiO_x$@CoO electrode at a current density of 1 A $g^{-1}$.

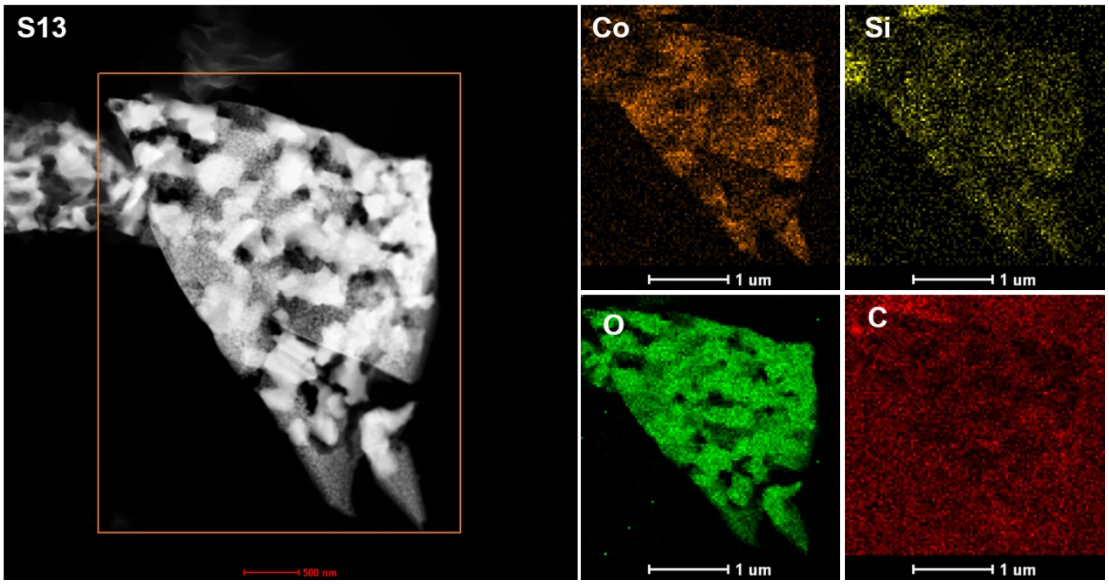


Figure S13: STEM HAADF images and the corresponding EDX elemental mappings of C, O, Si, and Co in $SiO_x$@C@CoO.

## Reference


[S1] Z. Y. Sang, Z. H. Zhao, D. Su, P. S. Miao, F. R. Zhang, H. M. Ji and X. Yan, *J. Mater. Chem. A*, 2018, **6**, 9064-9073.

[S2] Z. L. Li, H. L. Zhao, P. P. Lv, Z. J. Zhang, Y. Zhang, Z. H. Du, Y. Q. Teng, L. N. Zhao and Z. M. Zhu, *Adv. Funct. Mater.*, 2018, **28**, 1605711.

[S3] M. S. Han and J. Yu, *J. Power Sources*, 2019, **414**, 435-443.

[S4] Y. X. Liu, J. J. Ruan, F. Liu, Y. M. Fan and P. Wang, *J. Alloy Compd.*, 2019, **802**, 704-711.

[S5] D. Liu, C. R. Chen, Y. Y. Hu, J. Wu, D. Zheng, Z. Z. Xie, G. W. Wang, D. Y. Qu, J. S. Li and D. Y. Qu, *Electrochim. Acta*, 2018, **273**, 26-33.

[S6] W. He, Y. J. Liang, H. J. Tian, S. L. Zhang, Z. Meng and W. Q. Han, *Energy Storage Mater.*, 2017, **8**, 119-126.

[S7] W. J. Zhang, Y. Q. Weng, W. C. Shen, R. T. Lv, F. Y. Kang and Z. H. Huang, *Carbon*, 2020, **158**, 163-171.

[S8] J. L. Cui, H. B. Zhang, Y. Y. Liu, S. H. Li, W. X. He, J. L. Hu, and J. C. Sun, *Electrochim. Acta*, 2020, 334.

[S9] X. T. Guo, Y. Z. Zhang, F. Zhang, Q. Li, D. H. Anjum, H. F. Liang, Y. Liu, C. S. Liu, H. N. Alshareef and H. Pang, *J. Mater. Chem. A*, 2019, **7**, 15969-15974.

[S10] W. J. He, T. F. Zhang, J. M. Jiang, C. L. Chen, Y. D. Zhang, N. Liu, H. Dou and X. G. Zhang, *Acs Appl. Energ. Mater.*, 2020, **3**, 4394-4402.

[S11] M. H. Xu, J. J. Ma, G. L. Niu, H. X. Yang, M. F. Sun, X. C. Zhao, T. Y. Yang, L. Z. Chen and C. H. Wang, *Acs Omega*, 2020, *5*, 16440-16447.

[S12] L. Y. Chen, J. Zheng, S. Y. Lin, S. Khan, J. L. Huang, S. H. Liu, Z. R. Chen, D. C. Wu and R. W. Fu, *Acs Appl. Energ. Mater.*, 2020, **3**, 3562-3568.

[S13] K. Y. Zhang, H. Z. Mao, X. Gu, C. H. Song, J. Yang and Y. T. Qian, *Acs Appl. Mater. Inter.*, 2020, **12**, 7206-7211.

[S14] Z. X. Long, R. S. Fu, J. J. Ji, Z. Y. Feng, and Z. P. Liu, Chemnanomat, 2020, **6**, 1127-1135.

[S15] K. Pan, F. Zou, M. Canova, Y. Zhu and J. H. Kim, *J. Power Sources*, 2019, **413**,

20-28.

[S16] J. K. Dora, D. Nayak, S. Ghosh, V. Adyam, N. Yedla and T. K. Kundu, *Sustain Energ. Fuels*, 2020, **4**, 6054-6065.